Orientation of the intra-unit-cell magnetic moment in the high- T c superconductor HgB a_2 CuO_4+δ

Yang Tang, Lucile Mangin-Thro, Andrew Wildes, Mun Chan, Chelsey Dorow, Jaehong Jeong, Yvan Sidis, Martin Greven, Philippe Bourges

Orientation of the intra-unit-cell magnetic moment in the high-T_{c} superconductor HgBa_{2}CuO_{4+δ}

Yang Tang, Lucile Mangin-Thro, Andrew Wildes, Mun K. Chan, Chelsey J. Dorow, Jaehong Jeong, Yvan Sidis, Martin Greven, and Philippe Bourges

Phys. Rev. B **98**, 214418 — Published 12 December 2018

DOI: 10.1103/PhysRevB.98.214418

Orientation of the intra-unit-cell magnetic moment in the high-T_c superconductor $HgBa_2CuO_{4+\delta}$

Yang Tang[1], Lucile Mangin-Thro[2], Andrew Wildes[2], Mun K. Chan[1], Chelsey J. Dorow[1], Jaehong Jeong[3], Yvan Sidis[3], Martin Greven[1,*], Philippe Bourges[3,*]

[1] *School of Physics and Astronomy, University of Minnesota, Minneapolis, MN 55455, USA*

[2] *Institut Laue-Langevin, 71 avenue des martyrs, Grenoble 38000, France*

[3] *Laboratoire Léon Brillouin, CEA-CNRS, Université Paris-Saclay CEA-Saclay, Gif sur Yvette 91191, France*

* greven@umn.edu, philippe.bourges@cea.fr

Abstract

Polarized-neutron diffraction (PND) experiments have revealed that the pseudogap state of the cuprates exhibits unusual intra-unit-cell (IUC) magnetism. At a qualitative level, the data indicate a moment direction that is neither perpendicular nor parallel to the CuO_2 layers, yet an accurate measurement at a high-symmetry momentum point in a structurally simple compound has been lacking. Such a measurement would be crucial, as it would help to narrow down the scenarios for the microscopic origin of the IUC magnetism. Here we report PND results with unprecedented accuracy for the IUC magnetic order in the simple-tetragonal single-CuO_2-layer compound $HgBa_2CuO_{4+\delta}$. At the pseudogap temperature, we find evidence for magnetic critical scattering. Deep in the ordered state, we determine the moment direction to be 70° ± 10° away from the normal to the CuO_2 layers, which rules out both purely planar loop currents and high-symmetry Dirac multipoles, the two most prominent theoretical proposals for the microscopic origin of the IUC magnetism. However, the data are consistent with Dirac multipoles of lower symmetry or, alternatively, with a particular configuration of loop currents that flow on the faces of the CuO_6 octahedra.

I - Introduction

The lamellar high-temperature superconducting cuprates exhibit unusual properties as a result of their strong quasi-two-dimensional electronic correlations. One of the most interesting characteristics of these complex oxides is the pseudogap phenomenon, whose origin has been under intense debate [1]. Numerous experiments indicate that the pseudogap state is a distinct phase of matter, including circularly-polarized photoemission [2], polarized-neutron diffraction [3-12], polar Kerr effect [13], resonant ultrasound [14], optical birefringence [15], second-harmonic-generation optical response [16], torque magnetometry [17], and muon spin relaxation (μSR) [18]. The PND experiments span four different cuprate families and point to unusual IUC magnetic order (reduced wave vector $\mathbf{q} = 0$) that preserves the lattice translational symmetry. The IUC magnetic signal is observed below a doping-dependent characteristic temperature (denoted as either $T_{q=0}$ or T_{mag}) that matches the characteristic pseudogap temperature (T^*) determined from planar resistivity measurements (Fig. 1a) [19, 20]. This demonstrates that the IUC magnetic order is one of the hallmarks of the pseudogap phase. In the underdoped part of the phase diagram, the IUC magnetic order precedes the superconductivity and other electronic instabilities, such as charge-density-wave order (Fig. 1a). In the quantum-critical-point scenario of the cuprate phase diagram, fluctuations of this order parameter give rise to pairing and superconductivity [21-23].

Since the IUC magnetic order does not produce a net magnetization, it can be naively thought of as a simple superposition of an even number of moments that cancel out within each primitive cell. A state that gives rise to such magnetism was actually theoretically predicted [22,23] prior to the experimental findings. In this 'loop-current' (LC) model, spontaneous LCs develop within each square Cu-O plaquette. Orbital magnetism may arise from either two or four counter-circulating LCs per plaquette. The PND data are qualitatively consistent with the two-LC scenario [3-12], which is also supported by variational Monte Carlo calculations [24]. Whereas in the original model the orbital moments point perpendicular to the CuO_2 planes, the PND data indicate a significant in-plane component, albeit with rather large experimental uncertainty [3, 5, 6, 9, 10]. In a revised version of the original planar LC model, it was argued that such a magnetic signal might originate from a quantum superposition of (classical) LC

patterns [25]. Alternatively, the LCs might flow on the faces of the CuO_6 octahedra that surround Cu sites in a single-CuO_2-layer material such as $HgBa_2CuO_{4+\delta}$ (Hg1201), or on the faces of the CuO_5 pyramids in double-layer compounds such as $YBa_2Cu_3O_{6+x}$ (YBCO) [4,26-28]. Two distinctly different microscopic pictures involve planar oxygen moments [3] and Dirac (or magneto-electric) multipoles [29-31]. In order to help distinguish among these scenarios it is of considerable importance to determine the orientation of the IUC moments at the high-symmetry momentum point $\mathbf{Q} = (1,0,0)$ with higher precision. In particular, at non-zero values of the momentum transfer perpendicular to the copper-oxygen layers ($L \neq 0$), the neutron cross section mixes in-plane and out-of-plane components of the magnetic moment, which is undesirable. Moreover, this experiment ought to be performed in a structurally simple cuprate compound like Hg1201, which is free of possible ambiguities that may result from low structural symmetry and multiple adjacent CuO_2 layers. For example, systems with double-layer structure may exhibit additional *a*/*b* anisotropy [11] which prevents straightforward discussion of theoretical models [22-35], as the latter solely consider a single CuO_2 layer.

Whereas the microscopic nature of the IUC magnetism remains an open question, its existence has been firmly established through PND experiments performed on four different cuprate families. Perhaps the most important theoretical question is the relation between the IUC order and the pseudogap. The original LC model [22,23] faces a problem, since it can explain the IUC/$\mathbf{q}$=0 order reported by various measurements, but not the opening of the pseudogap. However, it has been argued that this problem is circumvented if the order is not truly long-range [32]. On the other hand, it has been argued that topological order can open a pseudogap and give rise to an emergent LC phase with a symmetry consistent with the neutron experiments [33]. Furthermore, various models imply charge- or pair-density-wave instabilities, e.g., with a composite *d*-wave superconducting and charge-density wave state with emergent SU(2) symmetry [34,35]. In these models, the pseudogap can be viewed as a phase of fluctuating superconducting correlations, and T^* may be a crossover temperature. However, a preemptive phase that breaks both parity and time-reversal symmetry, such as the original LC phase, is expected at T^* [34]. A very recent proposal, which is based on the experimental facts that the pseudogap is spatially inhomogeneous [36] and that no large thermodynamic anomaly is observed at T^* [37], argues that the pseudogap formation is a percolative phenomenon associated with gradual inhomogeneous charge localization [38]. In this scenario, the IUC order is an

emergent phenomenon that does not significantly affect the electronic density of states at the Fermi level. In these latter models, IUC order is an important ingredient and occurs systematically at higher temperature, prior to subsequent instabilities. In the present paper, we wish to better characterize the IUC order in a model experimental system, with particular focus on the question how to describe this state in terms of either LCs or magnetic multipoles.

We report PND measurements for two Hg1201 samples (Fig. 1a), one moderately under-doped (superconducting transition temperature T_c = 71 K, hole doping level $p \approx 0.095$; denoted UD71) and one nearly optimally-doped (T_c = 95 K, $p \approx 0.127$; OP95). The use of polarized neutrons is required in order to discern relatively weak magnetic signal from strong underlying nuclear Bragg diffraction. Prior measurements on samples grown by the same method [39], such as X-ray scattering [40, 41], charge transport [19,20,42-44], optical spectroscopy [45-47], and inelastic neutron scattering [48, 49] indicate that Hg1201 can be considered a model cuprate compound. Neutron diffraction results for Hg1201 [4,7] are highly consistent with the original discovery of the IUC magnetic order in YBCO [3,5]. Hg1201 has a particularly simple structure (high tetragonal P4/mmm crystal symmetry, one CuO_2 layer per primitive cell, no Cu-O chains), exhibits relatively small disorder effects [19,42-44], and features an optimal T_c of about 97 K, the highest among all single-layer cuprates. Hg1201 thus is a very promising compound for the study of the pseudogap magnetism. Unlike the previous PND studies of Hg1201, which focused on (1 0 L) reflections with nonzero integer L [4,7], we choose the high-symmetry reflection (1 0 0) in the present work, as this enables improved polarization analysis. In particular, any wave vector $\mathbf{Q}$ = (H K L) with nonzero out-of-plane component L results in the measurement of a superposition of in-plane and out-of-plane magnetic moments, rendering them difficult to distinguish in the polarization analysis. Moreover, (H 0 0)-type reflections have a unit-cell structure factor for magnetic neutron diffraction that is identically zero for axial dipoles and uniquely sensitive to Dirac multipoles [31].

II – Experimental details

We studied two $HgBa_2CuO_{4+\delta}$ samples, each comprised of approximately 30 co-aligned single crystals (each sample with a total mass of about 2 g). The crystals were grown by a flux method [39] and subsequently subjected to a heat treatment [19] in order to achieve the desired T_c. The superconducting transition temperature for each sample was estimated by averaging magnetic

susceptibility data of individual crystals measured by Quantum Design, Inc., Magnetic Property Measurement System (MPMS). The result of this averaging is shown in Supplementary figure 1 [50]. We estimate T_c = 71 ± 3 K (sample labeled UD71) and T_c = 95 ± 3 K (sample labeled OP95). The UD71 sample was used in a previous neutron scattering study of the antiferromagnetic spin dynamics response [48]. At the (1 1 0) Bragg reflection, we determined full-width-at-half-maximum (FWHM) mosaics of 1.5º for UD71 and 2.5º for OP95. Measurements were carried out at temperatures that ranged from slightly above T_c up to about 450 K, the temperature up to which the glue used to mount crystals (GE varnish) was found to be stable.

Most of the spin-polarized neutron diffraction experiments were performed on the cold neutron multi-detector diffractometer D7 at the Institute Laue-Langevin, Grenoble, France. The experimental set-up of D7 was similar to that of a previous study of $YBa_2Cu_3O_{6+x}$ [10] and is described in detail in the Supplemental Materials [50]. Genuine magnetic scattering can be obtained through longitudinal polarization analysis using the classic XYZ-polarization analysis technique [3,5,8,10,11]. In order to minimize neutron absorption of Hg, the incident neutron beam was monochromated to a relatively long wavelength (incident neutron energy of E_i = 20 meV, incident wavelength 3.1 Å or wave vector $k_i \approx 2.02$ Å^{-1}).

Additional measurements were performed on the triple-axis spectrometer 4F1 at LLB/Orphée. This instrument, described elsewhere [3-9], is also equipped with polarized-neutron capabilities and XYZ longitudinal polarization analysis. An incident wave vector k_i = 2.57 Å^{-1} (E_i=13.7 meV) was chosen and higher harmonics neutron were removed by a pyrolithic graphite filter placed before the polarizing super-mirror. The final neutron energy and polarization are analysed with an Heusler crystal.

As previously discussed in detail [12,56], the main difficulty in such an experiment is the determination of the temperature dependence of the bare flipping ratio, R_0, which primarily depends of the given instrument but also of the sample itself (shape, mosaicity,..). Further, due to imperfections in the neutron optics, the polarization is slightly spatially inhomogenous. Therefore, R_0 inevitably evolves with temperature, because the sample is slightly displaced within the polarized beam when the temperature is changed [56]. In practice, one considers $1/R_0$, which is determined at a nuclear Bragg position where no magnetic signal is expected. On a triple-axis spectrometer, this can be achieved by using the same neutron path (analyzer/detector)

after the sample, and by moving the analyzer arm to Bragg positions where no magnetic signal is expected. This is generally not possible on D7 due to geometric constraints, and because each scattering angle is typically associated with a specific bender/detector set. Therefore, the triple-axis instrument allows for a better determination of thermal drift of $1/R_0$, which limits systematic errors in the magnetic intensity. The two rather distinct instruments – D7 and 4F1 – have different types of limiting factors. On D7, it is the inability to accurately determine the baseline of the inverse of the flipping ratio, which inevitably drifts with temperature, and thus causes a systematic error that precludes an accurate determination of the magnetic intensity in OP95. However, the OP95 data serve as an excellent reference for the underdoped sample. The statistical errors are better on D7 than on 4F1, which leads to a better accuracy in the determination of the tilt angle of the IUC magnetic moment. On 4F1, one can better determine the flipping ratio drifts with temperature by moving the analyzer arm to Bragg positions where the magnetic signal is not expected and/or was not seen in previous studies. This is not possible on D7 due to geometric constraints.

On both experiments, the Hg1201 samples were mounted in the (H 0 L) horizontal scattering plane. We quote the scattering wave-vector $\mathbf{Q} = H\mathbf{a}^* + K\mathbf{b}^* + L\mathbf{c}^* \equiv (H\ K\ L)$ in reciprocal lattice units, where $\mathbf{a}^* = \mathbf{b}^* = 1.62$ Å^{-1} and $\mathbf{c}^* = 0.66$ Å^{-1} are the approximate room-temperature values.

III - Results

In contrast to the previous reports of IUC magnetic order in Hg1201 [4,7], we primarily perform measurements on the multi-detector diffractometer D7 [10]. We observe magnetic signal only for (1 0 L)-type Bragg reflections, consistent with the prior work [4,7] (see supplementary Figure S4 [50]). Figure 2 shows the temperature dependence of the inverse of the flipping ratio, $1/R$, for both UD71 and OP95. $1/R$ is defined as the ratio of the measured spin-flip (SF) intensity to the measured non-spin-flip (NSF) intensity, and $i = \{X,Y,Z\}$ denotes the three neutron polarizations: $1/R_i = I_i^{SF} / I_i^{NSF}$. For OP95, $1/R_i(T)$ decreases in a gradual, monotonic fashion with decreasing temperature and can be described (below about 400 K) by a polynomial fit. This behaviour is consistent with the lack of any magnetic Bragg signal, which would be expected to lead to an increase with decreasing temperature. In contrast, $1/R_i$(T) for UD71 exhibits an upturn below $T_{q=0} = 360$ - 380 K. A magnetic signal is thus observed for UD71 and absent (or very small) for

OP95, in agreement with prior observations [4,7]. Furthermore, $1/FR_i(T)$ for UD71 noticeably depends on the polarization, with a maximum amplitude for the Y-polarization.

In order to describe this polarization dependence, we first decompose the IUC magnetic moment $\boldsymbol{m}$ into the three polarization directions. The magnetic moment is a superposition of moments along the reciprocal lattice basis, $m^2 = m_a^2 + m_b^2 + m_c^2$. Since Hg1201 has tetragonal symmetry, and hence $\boldsymbol{a}^*$ and $\boldsymbol{b}^*$ are equivalent, the in-plane components are equal: $m_a^2 = m_b^2$. We therefore can simply express the moment in terms of the in-plane component $\boldsymbol{m_{ab}}$, with $m_{ab}^2 = 2m_a^2$, and out-of-plane component $\boldsymbol{m_c}$, which are related to the total magnetic moment as $m^2 = m_{ab}^2 + m_c^2$. We define □ to be the angle between the $\boldsymbol{c}^*$-axis and the total magnetic moment $\boldsymbol{m}$: $tan(□)=m_{ab}/m_c$ (see Fig. 1b). The magnetic components are related to the magnetic intensity contributions M_i along the three polarization directions. In the SF channel, for **Q** = (1 0 0) [12]:

$$M_Z \propto m_c^2 \tag{1}$$

$$M_Y \propto \frac{1}{2} m_{ab}^2 + sin^2\alpha\, m_c^2 \tag{2}$$

$$M_X \propto \frac{1}{2} m_{ab}^2 + cos^2\alpha\, m_c^2 \tag{3}$$

where α is defined as the angle between the momentum transfer $\boldsymbol{Q}$ and the polarization direction X (Fig. S1b). In the limit where α = 0, the magnetic intensity follows the sum-rule $M_X = M_Y + M_Z$ discussed in our previous reports using longitudinal polarization analysis on triple-axis spectrometers [3-11]. On the diffractometer D7, α = 108.2º ± 5º for $\boldsymbol{Q}$ = (1 0 0) (see Supplemental Materials). The relations (1) - (3), which are specifically satisfied for magnetic scattering, show that the magnetic signal should be maximum in Y polarization, as indeed observed for UD71 (Fig. 2).

Prior PND work revealed an order-parameter-like temperature dependence [5,7] for the **q** = 0 magnetic moment, and we therefore write:

$$m_{ab,c}(T) = m_{ab,c}\left(1 - \frac{T}{T_{q=0}}\right)^{\beta} \tag{4}$$

with $T_{q=0}$ the onset of the **q** = 0 order and β the effective exponent that describes the observed power-law-like temperature dependence. The detailed, quantitative data analysis to extract the **q** = 0 magnetic signal is described the Supplemental Materials [50]. The data are analysed in two different ways, which both yield essentially the same result. Method 1 assumes that both UD71

and OP95 exhibit **q** = 0 magnetism on top of a SF background with the same linear temperature dependence. The fits to the data using Eqs. 1-4 with the same linear background are shown in Fig. S4(g-l). For UD71, we find $T_{q=0} = 370 \pm 30$ K, slightly higher than the characteristic temperature T^* obtained from planar resistivity measurements [19, 20] (Fig. 1), and $\beta \approx 0.25 \pm 0.05$, consistent with the prior data for Hg1201 [7] and YBCO [5]. The extracted values (obtained in arbitrary units; see also Table 1) of m_{ab}^2 and m_c^2 are 0.58 ± 0.14 a.u. and 0.20 ± 0.06 a.u., respectively, which corresponds to ϕ = 71° ± 10°. For OP95, on the other hand, the in-plane and out-of-plane moments are zero within error, with an upper limit of about 0.08 a.u. for both. This absence of a discernible magnetic Bragg signal is consistent with the previously reported result for a nearly optimally doped Hg1201 sample (T_c = 89 K, $p \approx 0.116$) [4].

Figure 3 shows the magnetic intensity obtained with Method 2, where we assume no discernible magnetic signal in OP95 and use this as a background reference for UD71 (see also the Supplemental Materials [50]). Importantly, the signal satisfies polarization analysis, which demonstrates its magnetic origin: the solid lines in Fig. 3 show the fit to (1) - (4) below $T_{q=0}$ ~ 360 K, with $\beta \approx 0.20 \pm 0.05$, consistent with the value obtained with Method 1. The values for m_{ab}^2 and m_c^2 are listed in Table 1 together with those obtained from Method 1. The two methods give consistent results, within error. We obtain $T_{q=0} \approx 360 \pm 30$ K for the mean value, consistent with T^* from planar resistivity measurements [19,20] (Fig. 1a).

One can estimate the signal strength in absolute units from a comparison with the intensity of the (1 0 0) nuclear Bragg peak, which is ~ 300 a.u. and calculated to be 4.6 barn based on the composition and crystal structure of Hg1201. Then, assuming that the magnetic signal is long-range, the total magnetic intensity $m^2 = m_{ab}^2 + m_c^2$ is found to be 9.4 ± 2 mbarn for UD71, consistent with previous estimation [4]. This results in an upper bound of ~1.7 mbarn for OP95 at **Q** = (1 0 0).

Further, we have performed complementary triple-axis data on OP95 to arrive at a better estimate of this upper bound value. Using XYZ longitudinal polarization analysis, we recall that the angle α between $\boldsymbol{Q}$ and X (Fig. S2 and Eq. 4-6) goes to zero for a triple-axis spectrometer as we can choose the X channel to correspond to the **P**//**Q** configuration. Thus, the full magnetic intensity is given by M_X. The polarization sum rule then reads: $M_X = M_Y + M_Z$. Figure 4 shows the temperature dependence of the **q** = 0 magnetic intensity at **Q** = (1 0 L). Measurements were performed with **P**//**Q** in the SF channel (where the magnetic signal is expected to be maximum).

The data were obtained using a bare flipping ratio reference, $1/R_0$, obtained at (2 0 0) and (0 0 4) where no magnetic signal is expected, and further averaged following ref. [10] for YBCO. The magnetic intensity at (1 0 L) is calibrated in absolute units using the intensity of the nuclear Bragg peaks (4.62 barns at L = 0 and 1.26 barns at L = 1 [4,7]). In Figs 4a-b, a magnetic signal appears below $T_{q=0} \sim 220$ K. This signal can be described using a characteristic order-parameter-like T-dependence, Eq. 7 (with $\beta = 0.25$). Converted to absolute units, the magnetic intensity is estimated to be ~2 mbarns at **Q** = (1 0 0) and ~0.5 mbarns at **Q** = (1 0 1). The value for **Q** = (1 0 0) is consistent with our upper bound from the D7 measurement. We therefore obtain consistent results, despite possible remaining systematic uncertainties in the determination of the reference of the bare flipping ratio. By reducing the systematic errors on the triple-axis instrument, we arrive at a more precise upper bound estimate.

Recent μSR measurements of $YBa_2Cu_3O_{6+x}$ [18] and $Bi_2Sr_2CaCu_2O_{8+\delta}$ [57] revealed slow magnetic fluctuations and critical slowing down in the pseudogap phase. Further, recent ^{63}Cu nuclear magnetic resonance (NMR) measurements of the bilayer Hg-based cuprate $HgBa_2CaCu_2O_{6+\delta}$ indicate ultraslow fluctuations specifically below T* [58], which suggests the existence of subtle generic low-energy fluctuations in the pseudogap state of cuprates. For Hg1201 such studies have not yet been performed; only the lack of a static magnetic signal on the apical oxygen site has been reported from NMR [59]. In $YBa_2Cu_3O_{6+x}$, the μSR longitudinal relaxation rate was found to go through a maximum at the temperature $T_{q=0}$ (or T_{mag}) [18], a characteristic of critical slowing down typically associated with a second-order phase transition. In a PND study of nearly-optimally-doped $YBCO_{6.85}$ [10], performed on the D7 diffractometer used in the present work, evidence for critical-like magnetic scattering was reported at **Q** = (0.88 0 0), i.e., off the Bragg position. In Fig. 5b, we reproduce these data by plotting the sum of all SF cross-sections, $\Sigma_{SF} = I_{SF}^X + I_{SF}^Y + I_{SF}^Z$. Consistent with the μSR relaxation rate [18], Σ_{SF} exhibits a peak at the onset temperature of the **q** = 0 magnetic order suggestive of critical slowing down.

In Fig. 5(a), we report, we report the same quantity determined at **Q** = (0.88 0 -0.11), for both UD71 and OP95. We find that Σ_{SF} displays in each sample a peak as well at a temperature close to the pseudogap temperature T*. This feature can also be seen from the first derivative of Σ_{SF} (Fig. S5b), which exhibits a sharp S-shape for both samples at the respective T*. In OP95, the anomaly is consistently observed near the same temperature $T_{q=0} \sim 220$ K identified from the magnetic intensity on the Bragg peaks (Fig. 4). Further, a complementary measurement of the

magnetic scattering was performed around **Q**=(0.9,0,0) on the triple-axis spectrometer 4F1 using XYZ polarization analysis. The quantity $\Delta_{SF} = 2I_{SF}^{x} - \left(I_{SF}^{y} + I_{SF}^{z}\right)$ was obtained via polarization analysis. We note that all background contributions cancel out in Δ_{SF} [10], such that only the magnetic contribution remains. Interestingly, a maximum appears also in Δ_{SF} near 220 K (Figure S6.a) in agreement with Fig. 5.a. It is worth to stress that although for each dataset the anomalous behavior occurs on a single point, the same phenomenon is observed for both Hg1201 samples (Fig. 5.a) and one YBCO sample (Fig. 5.b), precisely at the expected T*. Additional experimental work is needed to more accurately and systematically investigate the possibility of critical fluctuations.,

For UD71, the characteristic temperature of the maximum of Σ_{SF} is consistent with the longitudinal polarization analysis at the Bragg position (1 0 0) (Figs. 2-3). For OP95, one can define the temperature $T_{q=0}$ ~ 200-220 K from the anomalies in Fig. 4 and Fig. 5.a, although magnetic intensity was not discernible at the Bragg position on D7 (Fig. 2). We note that another aspect of the additional measurements of OP95 at the (1 0 0) and (1 0 1) reflections on 4F1 is that they are made with a coarser (about 2 times) **Q**-resolution than on D7. Therefore, in light of the observation for nearly optimally-doped $YBCO_{6.85}$ of short-range, rather than long-range magnetic order [10], the **q** = 0 magnetism in OP95 could be short-range as well. As a consequence, the magnetic response is redistributed throughout the Brillouin zone and not discernible at the (1 0 0) Bragg peak within the experimental conditions of the D7 instrument. These observations motivated us to search for a weak magnetic signal away from the (1 0 0) Bragg position. Figure 5c shows the difference between (H 0 -0.4) momentum scans in the SF channel across H = 1 obtained at 150 K (below $T_{q=0}$) and 225 K (above $T_{q=0}$) (The raw data are shown in Fig. S6b). Indeed, we are able to discern a net magnetic signal at H = 1, consistent with the existence of short-range IUC magnetic order in OP95. A rough estimate of the in-plane correlation length yields $\xi/\square \sim 5$, a value that is even shorter than for $YBCO_{6.85}$ [11].

IV. Discussion

Figures 2-5 demonstrate that the observation of a magnetic signal in the pseudogap state of UD71 is independent of the data analysis method and consistent with a second-order phase transition at $T_{q=0} = 360 \pm 30$ K, accompanied by magnetic critical fluctuations. The present results for Hg1201, obtained with unprecedented signal-to-noise ratio, confirm prior work which

employed a triple-axis spectrometer [3-11]. For OP95, the magnetic Bragg signal is at least one order of magnitude weaker than for UD71 (see Table 1). Nevertheless, evidence for critical fluctuations near $T_{q=0} = 210 \pm 30$ K (Figs. 4 & 5a) and for short-range correlations is observed. Overall, these estimates are consistent with previous results for Hg1201 [4,7] (Fig. 1b), and with results for YBCO, where a similar evolution from long-range three-dimensional magnetic correlations at low doping toward short-range two-dimensional correlations near optimal doping was observed [10]. We note that the relatively narrow fluctuation range implied by the data in Fig. 5 suggests that the value of β, as extracted from fits to the extended observed power-law-like temperature dependence, is an effective exponent rather than a true critical exponent.

For UD71, quantitative longitudinal polarization analysis at the (1 0 0) Bragg reflection yields in-plane and out-of-plane IUC magnetic components with unprecedented accuracy (Table 1). The moment direction is tilted away from the crystallographic $\boldsymbol{c}$ axis by $\phi = 70° \pm 10°$. This value is somewhat larger, yet consistent with those obtained for other cuprates (Table 2).

Our results (Table 1) allow us to rule out models with strictly in-plane (ϕ = 90°) or out-of-plane (ϕ = 0) IUC moments. Specifically, we can rule out all models where ϕ goes to 0 at L = 0, in particular the original planar LC model [22,23], and models where ϕ goes to 90° at L = 0, in particular the magneto-electric multipole scenarios with quadratic symmetry of refs. [29-31] in which the out-of-plane moment component is zero. However, we cannot rule out variations of these scenarios, either within the LC picture, where an in-plane component appears due to quantum superposition of LC patterns [25], or quadrupolar order with monoclinic symmetry [31,32]. The quadrupole lobes (or current loops) exhibit different spontaneous magnetic fields on opposite sides of a Cu atom. The neutron spin moment probes these different microscopic magnetic patterns, and the interference between them, and the corresponding cross section can be expected to be largest when the size of the quadrupole lobes (or current loops) is comparable to the neutron wavelength. An interesting scenario that might explain our data is the dual existence of planar LC order and magneto-electric quadrupoles, as both can be treated in a consistent manner [60].

Our result also is consistent with a variant of the LC model in which charge currents flow on the faces of the oxygen pyramids/octahedra (Fig. 5d). For Hg1201, this corresponds to an angle of about 64°, as calculated from lattice parameters [4]. Several variants of this scenario have been considered [4,26-28,61]. However, most of these variants are inconsistent with our

data at the high symmetry point, $L = 0$ [26,27]. Indeed, structure factor calculations show that the variants considered in [4,26-28,61] exhibit out-of-plane and in-plane components at different Bragg positions: only the out-of-plane component contributes to the (1 0 0) reflection whereas the in-plane component would result in intensity at (0 0 L) Bragg peaks, which has not been observed in experiment. Only the specific variant with two current loops depicted in Fig. 5d is consistent both with the neutron and Kerr-effect data [28,61]; in this scenario, the currents flow on opposite faces of the two pyramids that form the CuO_6 octahedra of Hg1201.

YBCO features pairs of CuO_5 pyramids associated with adjacent CuO_2 planes rather than CuO_6 octahedra associated with a single plane. The faces of the pyramids form an angle of about 59° [4] with the CuO_2 planes. According to earlier results for (twin free) underdoped YBCO [11], the out-of-plane magnetic scattering exhibits an *a*-*b* anisotropy, which is furthermore *L*-dependent. This feature can be accounted for by a crisscrossed stacking of planar LCs and eliminates as a possible origin of the out-of-plane magnetic scattering all magnetic patterns that do not break parity, such as magnetism on the oxygen sites. Further, the PND data for nearly optimally-doped YBCO show the absence of a tilt ($\phi = 0$) at high temperature, where IUC magnetic correlations develop, and that ϕ acquires a nonzero value of 40 ± 9° at $T_{q=0}$ [10]. This variation of ϕ as a function of temperature is consistent with a crossover from classical to quantum planar LC correlations [25], or with the coexistence of planar LC order and another form of IUC magnetic order (the latter controlling the in-plane magnetic scattering intensity). The tilt angle reflects the degree of admixture either of different kinds of IUC orders, or of planar and out-of-plane currents, which might change not only with temperature, but also with doping. In this regard, it is interesting to note that ϕ is quite large for the underdoped Hg1201 sample, reaching 70 ± 10°, whereas, for a nearly optimally-doped $Bi_2Sr_2CaCu_2O_{8+\delta}$ the angle can be as small as 20 ± 20° below $T_{q=0}$ (Table 2).

In conclusion, we have conducted a quantitative polarized-neutron diffraction study of the model cuprate Hg1201. Consistent with prior work, we observe robust $\mathbf{q} = 0$ magnetic order in the pseudogap state of a moderately-doped sample with $T_c \approx 71$ K, and evidence for short-range correlations in a nearly optimally-doped sample with $T_c \approx 95$ K. In the former case, analysis of the data obtained at the (1 0 0) reflection yields the estimate $\phi = 70° \pm 10°$ for the tilt direction of the magnetic moment away from *c*-axis. This estimate constitutes a significant

improvement over prior data and places new constraints on the microscopic origin of the observed intra-unit-cell magnetism.

Acknowledgements: The work at the University of Minnesota was funded by the Department of Energy through the University of Minnesota Center for Quantum Materials under DE-SC-0016371. We also acknowledge financial support at LLB from the projects UNESCOS (contract ANR-14-CE05-0007) and NirvAna (contract ANR-14-OHRI-0010) of the ANR. We acknowledge decisive discussions with Dalila Bounoua, Sergio di Matteo, Thierry Giamarchi, Stephen Lovesey, Mike Norman and Chandra Varma on the topic of this article.

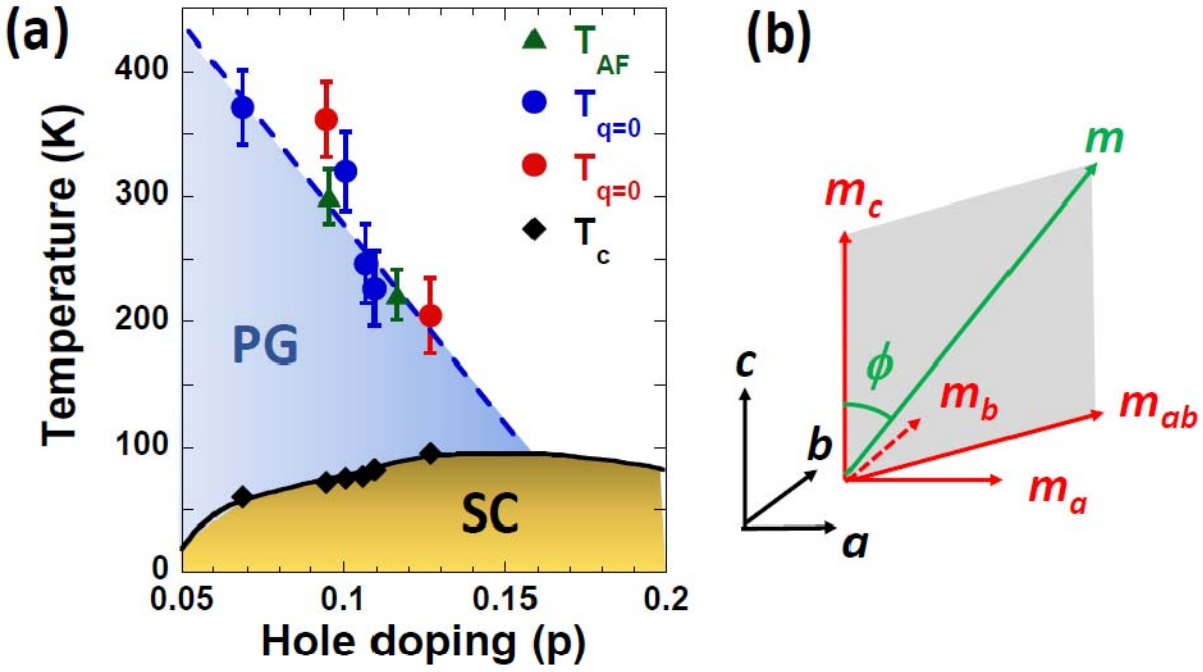

Figure 1. (a) Phase diagram of Hg1201, with superconducting (SC) and pseudogap (PG) phases. Red symbols pertain to the samples studied in the present work. The hole doping level (p) is determined from the $T_c(p)$ relationship according to [62]. Neutron scattering experiments reveal two characteristic temperatures associated with the PG phase: $T_{q=0}$ [4,7] and the onset temperature of the antiferromagnetic fluctuations T_{AF} [48, 49]. These temperatures are consistent with the characteristic pseudogap temperature T^* obtained from charge transport measurements [19, 20]. In an intermediate p-T range within the PG phase, charge order is reported below T_{CO} ($T_{CO} < T^*$) from X-ray [40, 41] and nonlinear optical [63] measurements (not shown). (b)

Definition of magnetic moment components; □ is defined as the angle between the *c*-axis and the total magnetic moment (***m***).

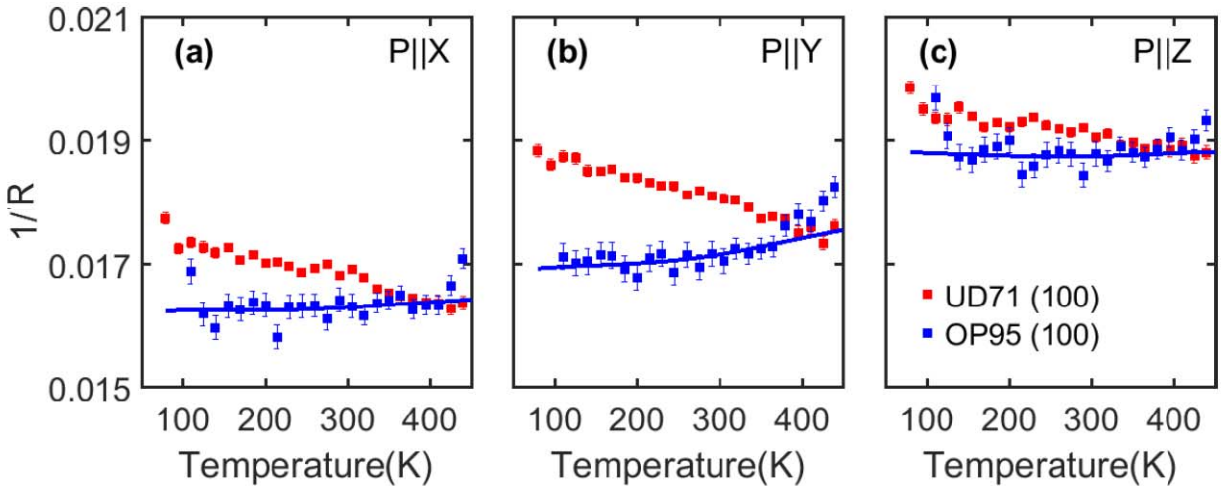

Figure 2. (a)-(c) Temperature dependence of the inverse flipping ratio (1/R) at the (1 0 0) reflection for the three polarization directions for UD71 (red) and OP95 (blue). A magnetic signal is evident in UD71 from the upturn below $T_{q=0}$ = 360 - 380 K. For better visualization, the OP95 results are shifted by ~ -0.004 (X) -0.005 (Y) and ~-0.003 (Z) to best match the average of the UD71 data between 360 and 400 K (above $T_{q=0}$). Solid blue lines are smooth polynomial fits to the OP95 data, with less weight given to the high-temperature data (~ 400 K and higher), where the uncertainty in the flipping ratio increases due to thermal effects on the sample mount that turned out to be larger than for the measurement of UD71.

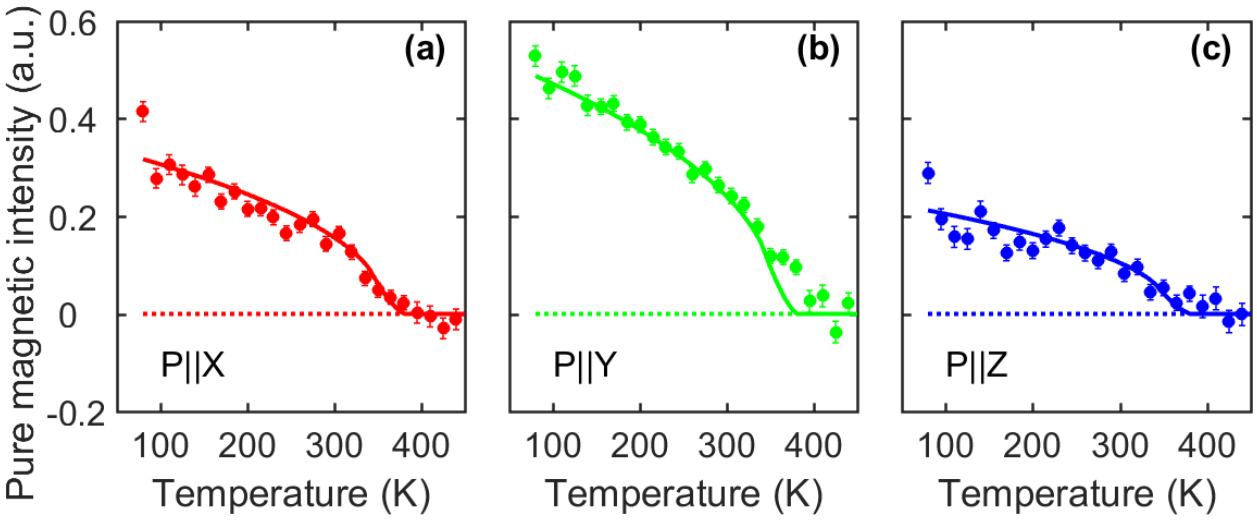

Figure 3 (a)-(c) Temperature dependence of the (1 0 0) magnetic signal for UD71 for the three polarization directions. The signal is extracted according to Method 2, which simply assumes that no discernible magnetic Bragg signal exists in OP95. The results to power-law fits are shown as solid lines.

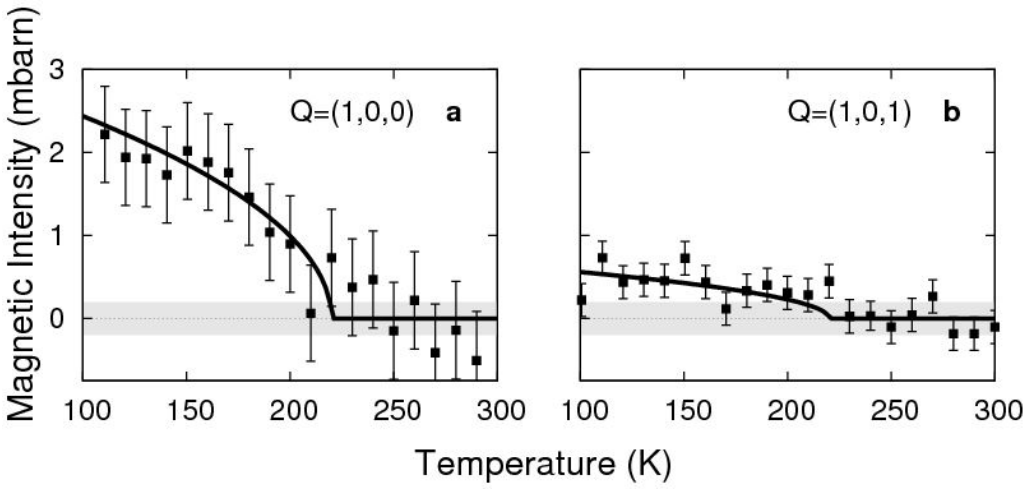

Figure 4 (a): Temperature dependence of the **q**=0 magnetic intensity extracted from measurements at the Bragg reflections **Q**=(1 0 *L*): (a) *L* = 0 and (b) *L* = 1. All the measurements were carried out with the **P**//**Q** configuration in the SF channel on the spectrometer 4F1 at LLB/Orphée on a OP95 sample that was very similar to the one measured on the D7 instrument at ILL (Fig. 2). Error bars are of standard deviation.

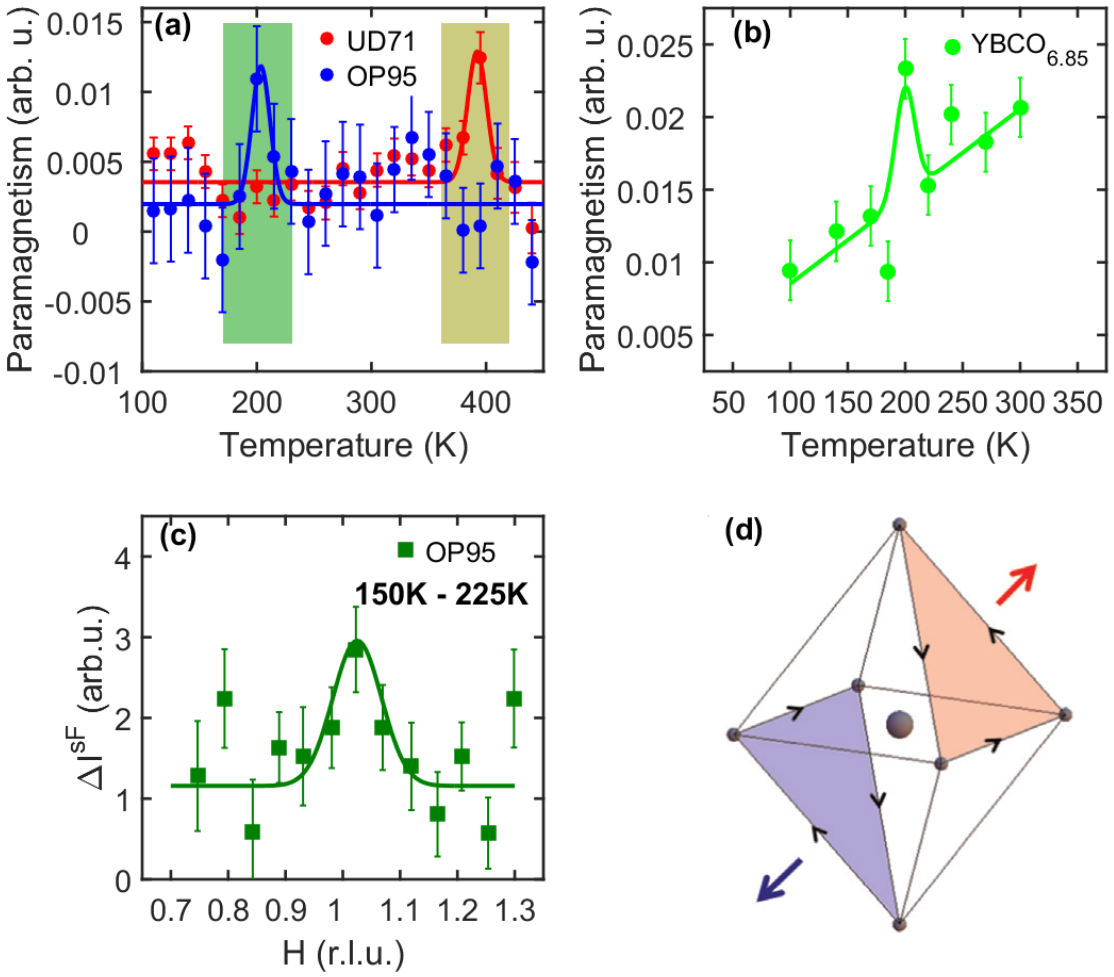

Figure 5 (a) Temperature dependence of $\Sigma_{SF} = I_{SF}^{x} + I_{SF}^{y} + I_{SF}^{z}$, the sum of the SF neutron cross-sections for the three polarization geometries. For both UD71 (red) and OP95 (blue), data are averaged over eleven momentum transfer values centered at **Q** = (0.88 0 -0.11) for better statistics. The peaks at ~ 370 K for UD71 and ~ 200 K for OP95, as highlighted by the yellow and green shaded areas, indicate the appearance of a magnetic signal away from the Bragg peak at a temperature consistent with the pseudogap temperature T^* obtained from transport measurements [20,42] (see Supplemental Materials [50] for data analysis details). (b) Temperature dependence of Σ_{SF} for $YBCO_{6.85}$ measured with the same spectrometer with a similar analysis method (from [11]). The data show a peak at ~ T^* as well. (c) Difference, Δ^{SF}, of **Q** = (H 0 -0.4) momentum scans for OP95 between T = 150 K and T = 225 K (see raw data in supplementary Fig. S6b [50]). (d) Schematic of non-planar LC order with currents along the faces of oxygen octahedra consistent with the data for Hg1201 [28].

Fitting Data	m_c^2 (a.u.)	m_{ab}^2 (a.u.)	$\phi = arctan\left(\frac{m_{ab}}{m_c}\right)$
UD71 Method 1	0.20 ± 0.06	0.58 ± 0.14	71° ± 10°
UD71 Method 2	0.24 ± 0.09	0.68 ± 0.16	69° ± 10°
OP95 Method 1	0.06 ± 0.08	0.04 ± 0.04	-

Table 1. Fit results for the square of the in-plane and out-of-plane components of the magnetic moment determined (in the same arbitrary units) from polarization analysis involving the (1 0 0) reflection. For UD71, the results for both analysis methods are shown, including the angle of the moment direction with respect to [0 0 1].

Compound [reference]	Sample T_c	Estimated tilt angle	L
$YBa_2Cu_3O_{6.6}$ [5]	61 K	35 ± 7° 55 ± 7°	0 1
$YBa_2Cu_3O_{6+x}$ [3]	54 K, 61 K, 64 K	45 ± 20°	1
$YBa_2Cu_3O_{6.85}$ [10]	89 K	40 ± 9°	0.25
$La_{1.915}Sr_{0.085}CuO_4$ [6]	22 K	~ 45°	0
$HgBa_2CuO_{4+\delta}$ [7]	75 K	45 ± 25°	1
$Bi_2Sr_2CaCu_2O_{8+\delta}$ [9]	85 K	20 ± 20°	3

Table 2. Summary of previous estimates of the tilt angle of the magnetic moment for various underdoped cuprates based on measurements at for **Q** = (1 0 *L*) [3, 5-7,9,10]. The estimated tilt angles all fall into the 45 ± 20° range.

References

[1] B. Keimer, S. A. Kivelson, M.R. Norman, S. Uchida and J. Zaanen, *Nature* **518**, 179 (2015)

[2] A. Kaminski, S. Rosenkranz, H. M. Fretwell, J. C. Campuzano, Z. Li, H. Raffy, W. G. Cullen, H. You, C. G. Oison, C. M. Varma, and H. Höchst, *Nature (London)* **416**, 610 (2002)

[3] B. Fauqué, Y. Sidis, V. Hinkov, S. Pailhès, C. T. Lin, X. Chaud, and P. Bourges, *Phys. Rev. Lett.* **96**, 197001 (2006)

[4] Y. Li, V. Balédent, N. Barišić, Y. Cho, B. Fauqué, Y. Sidis, G. Yu, X. Zhao, P. Bourges, and M. Greven, *Nature (London)* **455**, 372 (2008)

[5] H. A. Mook, Y. Sidis, B. Fauqué, V. Balédent, and P. Bourges, *Phys. Rev. B* **78**, 020506 (2008)

[6] V. Balédent, B. Fauqué, Y. Sidis, N. B. Christensen, S. Pailhès, K. Conder, E. Pomjakushina, J. Mesot, and P. Bourges. *Phys. Rev. Lett.* **105**, 027004 (2010)

[7] Y. Li, V. Balédent, N. Barišić, Y. C. Cho, Y. Sidis, G. Yu, X. Zhao, P. Bourges, and M. Greven, *Phys. Rev. B* **84**, 224508 (2011)

[8] P. Bourges and Y. Sidis, *C. R. Physique* **12**, 461 (2011)

[9] L. Mangin-Thro, Y. Sidis, P. Bourges, S. De Almeida-Didry, F. Giovannelli, and I. Laffez-Monot, *Phys. Rev. B* **89**, 094523 (2014)

[10] L. Mangin-Thro, Y. Sidis, A. Wildes and P. Bourges, *Nat. Commun.* **6**, 7705 (2015)

[11] L. Mangin-Thro, Yuan Li, Y. Sidis, and P. Bourges, *Phys. Rev. Lett.* **118**, 097003 (2017)

[12] Ph. Bourges, Y. Sidis, and L. Mangin-Thro, Phys. Rev B, **98**, 016501 (2018).

[13] J. Xia, E. Schemm, G. Deutscher, S. A. Kivelson, D. A. Bonn, W. N. Hardy, R. Liang, W. Siemons, G. Koster, M. M. Fejer, and A. Kapitulnik, *Phys. Rev. Lett.* **100**, 127002 (2008)

[14] A. Shekhter, B. J. Ramshaw, R. X. Liang, W. H. Hardy, D. A. Bonn, F. F. Balakirev, R. D. McDonald, J. B. Betts, S. C. Riggs and A. Migliori *Nature* **498**, 75-77 (2013)

[15] Y. Lubashevsky, L. Pan, T. Kirzhner, G. Koren, and N.P. Armitage, *Phys. Rev. Lett.* **112**, 147001 (2014).

[16] L. Zhao, C. A. Belvin, R. Liang, D. A. Bonn, W. N. Hardy, N. P. Armitage and D. Hsieh. *Nat. Phys.* **13**, 250-254 (2017)

[17] H. Murayama, Y. Sato, R. Kurihara, S. Kasahara, Y. Mizukami, Y. Kasahara, H. Uchiyama, A.Yamamoto, E.-G.Moon, J. Cai, J. Freyermuth, M. Greven, T. Shibauchi, and Y. Matsuda, preprint, arXiv:1805.00276

[18] Jian Zhang, Z. F. Ding, C. Tan, K. Huang, O. O. Bernal, P.-C. Ho, G. D. Morris, A. D. Hillier, P. K. Biswas, S. P. Cottrell, H. Xiang, X. Yao, D. E. MacLaughlin, Lei Shu, *Sci. Adv*., **4**, 5235 (2018)

[19] N. Barišić, Y. Li, X. Zhao, Y. C. Cho, G. Chabot-Couture, G. Yu, and M. Greven, *Phys. Rev. B* **78**, 054518 (2008)

[20] N. Barišić, M. K. Chan, Y. Li, G. Yu, X. Zhao, M. Dressel, A. Smontara and M. Greven, *Proc. Natl. Acad. Sci.* **110**, 12235 (2013)

[21] M.R. Norman, and C. Pépin, *Rep. Prog. Phys.* **66**, 1547 (2003)

[22] C. M. Varma, *Phys. Rev. B* **55**, 14554 (1997)

[23] C. M. Varma, *Phys. Rev. B* **73**, 155113 (2006)

[24] C. Weber, T. Giamarchi, and C. M. Varma, *Phys. Rev. Lett.* **112**, 117001 (2014)

[25] Y. He and C.M. Varma, *Phys. Rev. B* **86**, 035124 (2012)

[26] C. Weber, A. Läuchli, F. Mila, and T. Giamarchi, *Phys. Rev. Lett.* **102**, 017005 (2009)

[27] S. Lederer and S. A. Kivelson, *Phys. Rev. B* **85**, 155130 (2012)

[28] V. M. Yakovenko, *Physica B* **460**, 159-164 (2015)

[29] S. W. Lovesey, D. D. Khalyavin and U. Staub, *J. Phys.: Condens. Matter* **27**, 292201 (2015)

[30] M. Fechner, M. J. A. Fierz, F. Thöle, U. Staub and N. A. Spaldin, *Phys. Rev. B* **93**, 174419 (2016)

[31] S. W. Lovesey and D. D. Khalyavin, *J. Phys.: Condens. Matter* **29**, 215603 (2017)

[32] C. M. Varma, *J. Phys.: Condens. Matter*, **26**, 505701 (2014)

[33] S. Chatterjee and S. Sachdev, *Phys. Rev. B* **95**, 205133 (2017)

[34] D. F. Agterberg, Drew S. Melchert, and M. K. Kashyap, *Phys. Rev. B* **91**, 054502 (2015)

[35] C. Morice, D. Chakraborty, X. Montiel, and C. Pépin, *J. Phys.: Condens. Matter* **30**, 295601 (2018).

[36] J. W. Alldredge, K. Fujita, H. Eisaki, S. Uchida, and Kyle McElroy, *Phys. Rev. B* **87**, 104520 (2013)

[37] J.W. Loram, K.A. Mirza, J.R. Cooper, and W.Y. Liang, *Phys Rev Lett* **71**, 1740 (1993)

[38] D. Pelc, P. Popčević, G. Yu, M. Požek, M. Greven, N. Barišić, preprint, https://arxiv.org/abs/1710.10221

[39] X. Zhao, G. Yu, Y. Cho, G. Chabot-Couture, N. Barišić, P. Bourges, N. Kaneko, Y. Li, L. Lu, E. M. Motoyama, O. P. Vajk and M. Greven, *Adv. Mater.* **18**, 3243 (2006)

[40] W. Tabis, Y. Li, M. Le Tacon, L. Braicovich, A. Kreyssig, M. Minola, G. Dellea, E. Weschke, M. J. Veit, M. Ramazanoglu, A. I. Goldman, T. Schmitt, G. Ghiringhelli, N. Barišić, M. K. Chan, C. J. Dorow, G. Yu, X. Zhao, B. Keimer & M. Greven, *Nat. Commun.* **5**, 5875 (2014)

[41] W. Tabis, B. Yu, I. Bialo, M. Bluschke, T. Kolodziej, A. Kozlowski, E. Blackburn, K. Sen, E. M. Forgan, M. Zimmermann, Y. Tang, E. Weschke, B. Vignolle, M. Hepting, H. Gretarsson, R. Sutarto, F. He, M. Le Tacon, N. Barišić G. Yu, and M. Greven, *Phys. Rev. B* **96**, 134510 (2017)

[42] N. Barišić, S. Badoux, M. K. Chan, C. Dorow, W. Tabis, B. Vignolle, G. Yu, J. Béard, X. Zhao, C. Proust and M. Greven, *Nat. Phys.* **9**, 761 (2013)

[43] M. K. Chan, M. J. Veit, C. J. Dorow, Y. Ge, Y. Li, W. Tabis, Y. Tang, X. Zhao, N. Barišić and M. Greven, *Phys. Rev. Lett.* **113**, 177005 (2014)

[44] M. K. Chan, N. Harrison, R. D. McDonald, B. J. Ramshaw, K. A. Modic, N. Barišić & M. Greven, *Nat. Commun.* **7**, 12244 (2016)

[45] E. van Heumen, R. Lortz, A. B. Kuzmenko, F. Carbone, D. van der Marel, X. Zhao, G. Yu, Y. Cho, N. Barišić, M. Greven et al., *Phys. Rev. B* **75**, 054522 (2007)

[46] Seyed Iman Mirzaei, Damien Stricker, Jason N. Hancock, Christophe Berthod, Antoine Georges, Erik van Heumen, Mun K. Chan, Xudong Zhao, Yuan Li, Martin Greven, Neven Barišić, and Dirk van der Marel, *Proc. Natl. Acad. Sci.* **110**, 5774 (2013)

[47] E. van Heumen, E. Muhlethaler, A. B. Kuzmenko, H. Eisaki, W. Meevasana, M. Greven, and D. van der Marel, *Phys. Rev. B* **79**, 184512 (2009)

[48] M. K. Chan, C. J. Dorow, L. Mangin-Thro, Y. Tang, Y. Ge, M. J. Veit, G. Yu, X. Zhao, A. D. Christianson, J. T. Park, Y. Sidis, P. Steffens, D. L. Abernathy, P. Bourges and M. Greven, *Nat. Commun.* **7**, 10819 (2016)

[49] M. K. Chan, Y. Tang, C. J. Dorow, J. Jeong, L. Mangin-Thro, M. J. Veit, Y. Ge, D. L. Abernathy, Y. Sidis, P. Bourges and M. Greven, *Phys. Rev. Lett.* **117**, 277002 (2016)

[50] See Supplemental Material http://link.aps.org/... for experimental information and data analysis methods of the D7 (ILL) measurements which includes Refs. [51–55], additional measurements on the triple-axis 4F1 (LLB/Orphée) and supplementary figures.

[51] Stewart, J.R. *et al.*. *J. Appl. Cryst.* 42, 69-84 (2009).

[52] G. Ehlers, G. Stewart, J.R., Wildes, A.R., Deen, P.P. & Andersen, K.H., *Review of Scientific Instruments* **84**, 093901 (2013).

[53] T. Fennell, L. Mangin-Thro, H. Mutka, G.J. Nilsen and A.R. Wildes, Nucl. Inst. and Meth. Phys. Res. A **857** 24 (2017).

[54] M. Campostrini, M. Hasenbusch, A. Pelissetto, P. Rossi and E. Vicari. *Phys. Rev. B* **63**, 214503 (2001)

[55] V. Aji and C. M. Varma. *Phys. Rev. B* **79**, 184501 (2009)

[56] P. Bourges, D. Bounoua, J. Jeong, L. Mangin-Thro and Y. Sidis, preprint, arXiv:1810.08779.

[57] A. Pal, S.R. Dunsiger, K. Akintola, A. Fang, A. Elhosary, M. Ishikado, H. Eisaki, J. E. Sonier, *Phys. Rev. B* **97**, 060502 (2018)

[58] Y. Itoh, T. Machi, and A. Yamamoto, *Phys. Rev. B* **95**, 094501 (2017)

[59] A.M. Mounce, Sangwon Oh, W.P. Halperin, A.P. Reyes, P.L. Kuhns, M. Chan, J. Li, D. Xia, X. Zhao, and M. Greven, *Phys. Rev. Lett.* **111**, 187003 (2013).

[60] S. Di Matteo and M. Norman, *Phys. Rev. B* **85**, 253143 (2012)

[61] J. Orenstein, *Phys. Rev. Lett.* **107** 067002 (2011)

[62] A. Yamamoto, W.-Z. Hu, and S. Tajima, *Phys. Rev. B* **63**, 024504 (2000)

[63] J. P. Hinton, E. Thewalt, Z. Alpichshev, F. Mahmood, J. D. Koralek, M. K. Chan, M. J. Veit, C. J. Dorow, N. Barišić, A. F. Kemper, D. A. Bonn, W. N. Hardy, Ruixing Liang, N. Gedik, M. Greven, A. Lanzara, and J. Orenstein, Sci. Rep. **6**, 23610 (2016)